Validation of a Long-Range Trajectory Model Using Gas Balloon Tracks from the Gordon Bennett Cup 95

KATHRIN BAUMANN

Central Institute of Meteorology and Geodynamics, Vienna, Austria

ANDREAS STOHL

Institute of Meteorology and Physics, University for Agricultural Sciences, Vienna, Austria

(Manuscript received 18 July 1996, in final form 2 October 1996)

ABSTRACT

In September 1995, 18 gas balloon teams competed at the Gordon Bennett Cup, a long-distance ballooning event. The landing positions, travel times of all teams, and detailed information on the tracks of four teams are available. A special version of the trajectory model FLEXTRA (flexible trajectories) is used that allows the heights of calculated trajectories to be adjusted to the respective balloon heights at every computation time step. The comparison of calculated and observed balloon trajectories allows a validation of the trajectory model. In this case study, the agreement between calculated and balloon trajectories was good, with average relative transport errors of less than 20% of the travel distance after 46 h of travel time. Most of the trajectory errors originate from interpolation errors and from amplifications of small position disturbances in divergent wind fields. Trajectory ensembles, taking into account stochastic errors occurring during the trajectory calculations, are shown to be very reliable in assessing the uncertainties of the computed trajectories. In the present study, the balloon tracks were enveloped by the ensemble trajectories most of the time, suggesting that errors in the analyzed wind fields were relatively small.

1. Introduction

Trajectories are often used to describe the long-range transport of air pollutants in the atmosphere (Pack et al. 1978) and to establish source–receptor relationships of air pollutants (Miller 1987; Stohl 1996a,b). Therefore, there is a strong interest in assessing their accuracy and the magnitude of errors that occur from a variety of sources.

Truncation errors, the only errors that can be kept below any limit by using sufficiently small time steps, are caused by the numerical integration of the trajectory equation (Walmsley and Mailhot 1983; Seibert 1993).

Interpolation from a regular grid to the actual trajectory position is necessary both in space and time, causing interpolation errors. Their magnitude can be assessed by degrading high-resolution wind fields and comparing trajectories calculated from both the high-resolution and the low-resolution wind fields (Kuo et al. 1985; Rolph and Draxler 1990; Doty and Perkey 1993; Stohl et al. 1995). Trajectory position errors due to interpolation errors typically reach several hundred kilometers after 96 h of travel time. Interpolation errors are thus a major error source in the computation of trajectories. Stohl et al. (1995) suggested that ensembles of trajectories with random errors added at each time step be calculated to assess trajectory uncertainty caused by interpolation. Kahl (1996) used a similar method and defined the *meteorological complexity factor* as the mean distance between the reference and the stochastic trajectory locations.

Often, the starting position of a trajectory—as in the case of an accidental release—is poorly defined. Initially small position errors can amplify in diffluent wind fields, causing substantial trajectory uncertainties. Merrill et al. (1985) assessed this type of error by starting an ensemble of trajectories from slightly different positions.

Maryon and Heasman (1988) examined the effect of forecast errors by comparing forecasted to analyzed trajectories. They found that errors of forward trajectories that started at the beginning of the forecast period were relatively small, but errors of trajectories started 36 h into the forecast were substantial. Kahl and Samson (1986) used observation networks of different density and found that large errors occur from the interpolation of radiosonde measurements. These errors significantly affect the accuracy of trajectories. Kahl et al. (1989) compared trajectories at 850 and 700 hPa, calculated

Corresponding author address: Kathrin Baumann, Dept. of Environmental Meteorology, Central Institute of Meteorology and Geodynamics, Hohe Warte 38, A-1190 Vienna, Austria.
E-mail: kathrin.baumann@zamg.ac.at

from analyzed fields provided by the European Centre for Medium-Range Weather Forecasts (ECMWF) and by the National Meteorological Center (currently known as the National Centers for Environmental Prediction), and found a median separation of 1000 km after 120 h of travel time. In a similar study above the South Atlantic, a region with scarce observational data, Pickering et al. (1994) found average separations of 1500 km after 120 h of travel time and 2500 km after 192 h of travel time, corresponding to some 60% of the distances traveled.

Further trajectory errors are related to different assumptions in the treatment of vertical velocity. Vertical motions can be neglected (e.g., isobaric trajectories), assumed to be adiabatic (e.g., isentropic trajectories), or explicitly accounted for using dynamically balanced velocities from a numerical weather prediction model (three-dimensional trajectories). The third approach is physically most sensible, but due to its high-frequency variations, interpolation of the vertical wind component involves severe interpolation errors. Intercomparisons of several trajectory types have been presented by Kuo et al. (1985), Haagenson et al. (1987, 1990) and Stohl et al. (1995). Average deviations of typically 10%–30% of the travel distance were found.

All previously discussed error sources contribute to the total error of a trajectory. The only possible way to assess its total error is to compare it with the ''true'' trajectory. In doing so, the difficulty is obviously to determine this true trajectory. Generally, a tracer must be found to tag an air parcel.

Unfortunately, few tracers are suited to trace the real air motion. Conservative dynamic quantities such as potential vorticity (Artz et al. 1985), as well as material tracers such as Saharan dust (Martin et al. 1990), smoke from the oil fires in Kuwait (McQueen and Draxler 1994), and nonreactive gases and radioactive emissions from Chernobyl (Klug 1992), have been used. Reliable error assessments offer planned releases of tracer gases, as done during the Cross-Appalachian Experiment (CAPTEX) (Haagenson et al. 1987) and Across North America Tracer Experiment (ANATEX) (Haagenson et al. 1990), and the release of constant-level balloons (tetroons) (e.g., Reisinger and Mueller 1983; Knudsen and Carver 1994) or other balloons (Stocker et al. 1990; Kahl et al. 1991; Stohl et al. 1997). During CAPTEX, trajectory errors were approximately 25% of the mean transit distance after 24 h (Haagenson et al. 1987). Similar errors were found for ANATEX data (Haagenson et al. 1990), but the relative error decreased somewhat with travel time, yielding smaller relative errors after 72 h. Using a different method, Draxler (1991) found errors of 20%–30% for the same dataset. A case with a very small trajectory error was reported by Reiff et al. (1986), who investigated an episode of Saharan dust transport to Europe. The transport error of their three-dimensional trajectory was less than 200 km after a travel distance of 3000 km.

Most of the reliable tracer-derived data are restricted to relatively short travel times and distances. The tracer data of ANATEX, one of the largest tracer experiments suited for investigating trajectory errors up to this time, allow assessments of trajectory accuracy up to 72 h of travel time. Tracer experiments on that scale, however, are very expensive, and thus few data are available.

Gas balloon data have not often been used to assess trajectory errors. Draxler (1996) compared the track of a solo transpacific balloon flight to trajectories computed at different pressure levels. He demonstrated that forecast trajectories may be used for balloon flight planning. In this paper, a new possibility for investigating the accuracy of long-range trajectories is presented. In the framework of an international long-distance ballooning competition, tracks of gas balloons with travel times of up to 4 days were recorded. Gas balloons are manned airships filled with hydrogen. The pilot sheds ballast to make the balloon rise or lets out gas to make it sink. As far as horizontal movements are concerned, the gas balloon is borne along passively in the air current. We used the gas balloons as tracers of horizontal air motions and compared their tracks to trajectories computed at heights that varied in accordance with the ascending and descending motions of the balloons.

2. The Gordon Bennett Cup 1995

a. The balloon tracks—Available data

The 39th Gordon Bennett Cup,[1] a long-distance ballooning competition, was held with takeoff at 2030 UTC 9 September 1995 in Wil, Switzerland. Eighteen ballooning teams took part in the competition. The winning team (hereafter referred to as team 1) covered a distance of 1628 km within 92 h. An overview of the covered distances, the travel times, and mean speeds of all balloons is given in Table 1. The average of the mean speeds of all teams was 5 m s^{-1}.

The spatial distribution of the landing points of all teams (Fig. 1) demonstrates the variety of directions and distances flown by the balloons. In spite of a constant westerly upper-level flow, the balloon tracks differed widely because of their different travel heights, ranging from 500 m to more than 5000 m above sea level (ASL).

Detailed data of balloon heights and positions along the tracks were only available for teams 1, 3, 6, and 7. The horizontal position of the gas balloon of team 3 was determined with the Global Positioning System, while those of the other teams were reconstructed manually from verbal position information supplied by the pilots. The vertical positions were computed from air pressure readings.

Trajectories derived from balloon flights provide a

[1] James Gordon Bennett (1841–1918) was a donator to several sportive events.

TABLE 1. Distance between starting and landing position (LR), flight time, and resulting mean travel speed of all teams, ranked according to the distance covered.

Team	LR (km)	Flight time (h)	Mean speed (m s^{-1})
1	1628	92	5.0
2	1403	69	5.6
3	1395	81	4.8
4	1280	65	5.4
5	1267	62	5.6
6	931	46	5.6
7	906	48	5.3
8	872	35	6.9
9	839	42	5.5
10	805	45	5.0
11	625	55	3.1
12	499	22	6.2
13	495	26	5.2
14	297	13	6.2
15	251	23	3.1
16	220	7	8.5
17	137	14	2.7
18	52	8	1.8

good opportunity to validate computed trajectories, but there are also some limitations. The vertical displacement of a gas balloon is actively driven by the pilot and is therefore not related to the vertical wind component. Balloon tracks are thus not representative of three-dimensional airmass trajectories, but only allow the investigation of trajectory errors caused by errors in the horizontal wind components.

Another uncertainty arises from the temporal frequency of the balloon height data. Especially for team 6, the height information was given infrequently, with periods of several hours of missing data. Height information from teams 1, 3, and 7 was available at least once every 1 or 2 h.

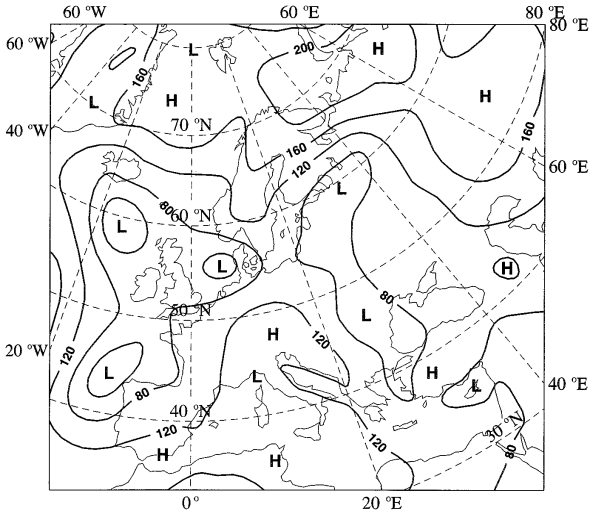

FIG. 2. ECMWF analysis of the geopotential field at 1000 hPa for 0000 UTC 10 September.

b. The synoptic situation

High-index zonal flows with embedded frontal systems dominated the circulation over all of Europe during the first half of September 1995. The 1000-hPa geopotential field of 0000 UTC 10 September (Fig. 2) shows cyclonic systems over the eastern Atlantic, over the North Sea, and west of the Urals. High pressure influence extended from southern Europe toward the Alps. This pressure pattern resulted in southerly winds at the western edge of the Alps and westerly winds in the north of central Europe. At 500 hPa (Fig. 3), westerlies dominated over southern Europe. A trough was situated above the eastern Balkan.

During the following days, a weakening of the pressure gradient resulted in generally weak surface winds in central Europe. The trough in the upper geopotential

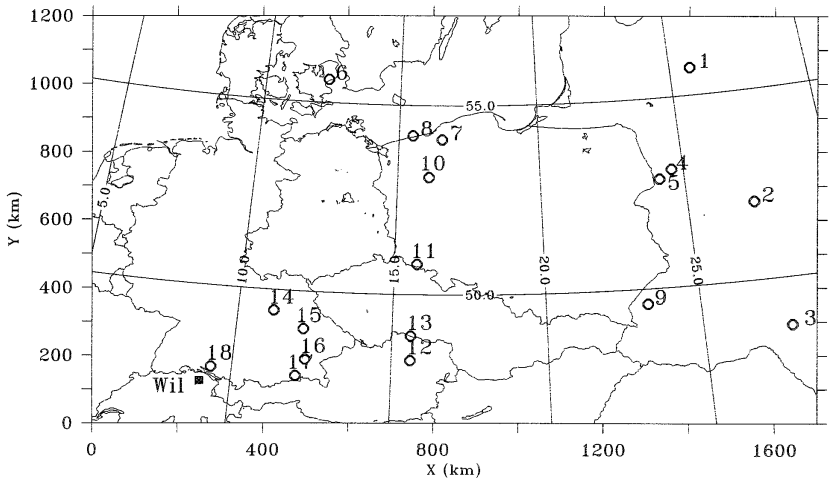

FIG. 1. Starting and ending positions of all the balloon teams.

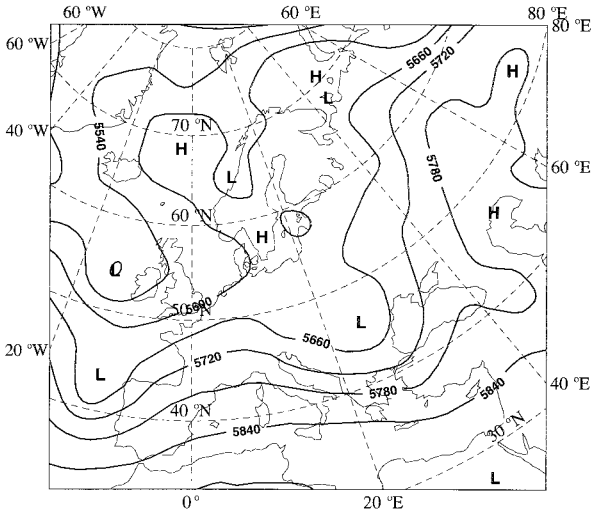

FIG. 3. ECMWF analysis of the geopotential field at the 500-hPa pressure level for 0000 UTC 10 September.

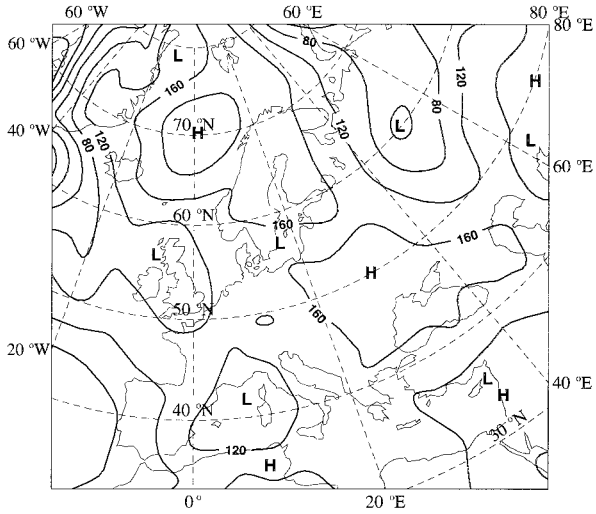

FIG. 4. ECMWF analysis of the geopotential field at 1000 hPa for 0000 UTC 13 September.

field moved eastward across the Black Sea, and the upper pressure gradients became weaker as well.

On 13 September, the surface pressure pattern (Fig. 4) showed weak pressure gradients all over Europe, with a continental high pressure area above eastern Europe. This resulted in weak, but highly variable, surface winds. On the 500-hPa chart (Fig. 5), a blocking anticyclone was located east of Iceland, but the westerlies still prevailed above eastern Europe.

3. Model description and method of validation

a. The model FLEXTRA

For the trajectory calculations, forecast and analysis data of the T213 L31 model from the European Centre for Medium-Range Weather Forecasts (ECMWF 1995) were available on the 31 model levels on a 1.0° resolution grid. Analysis (at 0000, 0600, 1200, and 1800 UTC) and first-guess (i.e., short-range forecasts at 0300, 0900, 1500, and 2100 UTC) data supplied by the ECMWF every 3 h were used to calculate diagnostic trajectories. Forecast trajectories were based on ECMWF forecast data available every 6 h.

Trajectories were computed with the kinematic trajectory model FLEXTRA (flexible trajectories) (Stohl et al. 1995). Depending on the available data, it is possible to compute several different trajectories (three-dimensional, constant model level, isentropic, isobaric, and boundary layer trajectories). For the numerical integration, the iterative scheme described by Petterssen (1940) is used. The FLEXTRA model uses a flexible integration time step Δt, which must fulfill the Courant–Friedrichs–Lewy (CFL) criterion $C < 1$ (recommended $C = 0.2$) with $C = v_i \Delta t / \Delta x_i$, where Δx_i are the grid distances and v_i are the wind components in horizontal and vertical directions, respectively. We used bicubic interpolation in the horizontal, quadratic interpolation in the vertical, and linear interpolation in time.

Gas balloons drift with the horizontal flow, but they sink because of downdrafts, radiative cooling, loosing hydrogen, or wetting of the balloon envelope, and they rise because of updrafts, solar warming, or dropping ballast. Thus, none of the usual trajectory types can represent their paths correctly. Therefore, a special feature of the FLEXTRA model was developed that allowed the altitudes ASL of the computed trajectories to be adjusted to those of the balloons. Thus, the altitude of the calculated trajectory was identical to that of the respective balloon trajectory at every computational time step. When the altitude of the balloon was below that of the lowest model level (e.g., in mountainous

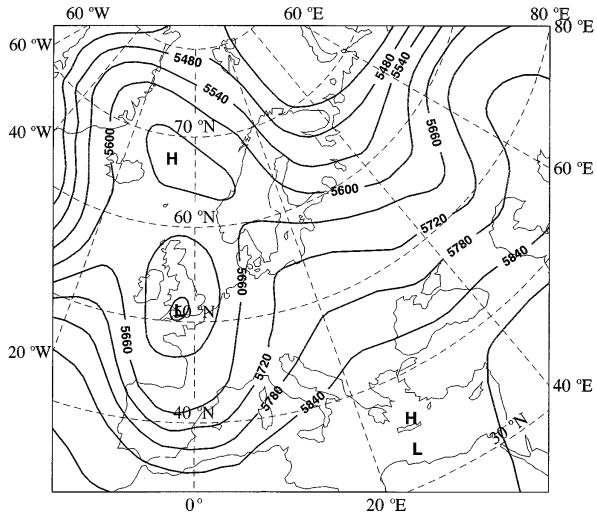

FIG. 5. ECMWF analysis of the geopotential field at the 500-hPa pressure level for 0000 UTC 13 September.

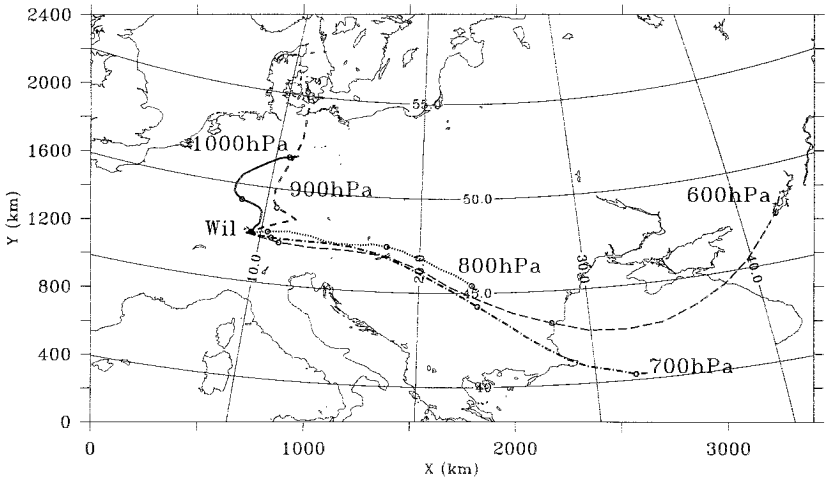

FIG. 6. Isobaric trajectories at the surface and at 900, 800, 700, and 600 hPa, based on ECMWF forecasts, starting at 2000 UTC 9 September at Wil, Switzerland. Trajectory positions are marked every 24 h.

areas), the wind at the lowest model level was used for the trajectory calculation.

Vertical motions were not computed by the trajectory model, but were prescribed by the height variations of the balloons. We limited the integration time step to 10 min. This guaranteed that, in general, the trajectories did not cross more than one model level within a single time step during the ascents or descents of the balloons. We linearly interpolated the heights of the balloons to these short time steps.

b. Measures of trajectory differences

Several important characteristics of the trajectories were considered to compare calculated and balloon trajectories: the total pathlengths along the tracks LP, the distances between starting and landing points (range LR), the total travel times T, and the maximum and mean balloon heights. The average balloon speed is given by LP/T. In accordance with Reisinger and Mueller (1983), we refer to

$$\mathrm{MF} = \frac{\mathrm{LP}}{\mathrm{LR}} \tag{1}$$

as the ''meandering factor.''

Absolute and relative horizontal transport deviations (AHTD, RHTD) have been used by some authors to quantify inaccuracies of calculated trajectories (Kuo et al. 1985; Rolph and Draxler 1990; Stohl et al. 1995). The absolute horizontal transport deviation was defined as

$$\mathrm{AHTD}(t) = \frac{1}{N}\sum_{n=1}^{N} \{[X_n(t) - x_n(t)]^2 + [Y_n(t) - y_n(t)]^2\}^{1/2}, \tag{2}$$

where N is the number of trajectories used (i.e., $N = 1$ for the detailed comparisons presented below), X and Y are the locations of the balloon trajectory, and x and y are the locations of the calculated trajectory at travel time t.

In addition, the relative horizontal transport deviation was introduced as

$$\mathrm{RHTD}(t) = \frac{1}{N}\sum_{n=1}^{N} \frac{\{[X_n(t) - x_n(t)]^2 + [Y_n(t) - y_n(t)]^2\}^{1/2}}{\mathrm{LH}_n(t)}, \tag{3}$$

with the mean trajectory length

$$\begin{aligned}\mathrm{LH}_n(t) = \frac{1}{2}\sum_{t_i=1}^{t} &\{[X_n(t_i) - X_n(t_{i-1})]^2 \\ &+ [Y_n(t_i) - Y_n(t_{i-1})]^2\}^{1/2} \\ &+ \{[x_n(t_i) - x_n(t_{i-1})]^2 \\ &+ [y_n(t_i) - y_n(t_{i-1})]^2\}^{1/2}.\end{aligned} \tag{4}$$

General previous findings concerning trajectory errors are that the AHTD increases with travel time, whereas the RHTD decreases (e.g., Haagenson et al. 1990).

4. Results

a. Isobaric forecast and analysis trajectories

To support the Austrian balloonists (team 3), isobaric forecast trajectories at the surface and at the 900-, 800-, 700-, and 600-hPa levels were calculated based on the ECMWF model run of 1200 UTC 8 September (T + 32 h). Prognostic wind fields were available up to T + 84 h. Forward trajectories were started at the same time and place as the balloons and calculated 52 h into the future (Fig. 6). The lowest trajectories (surface and 900 hPa) illustrated the highly variable winds caused by the weak gradients of the anticyclonic pressure field at these levels.

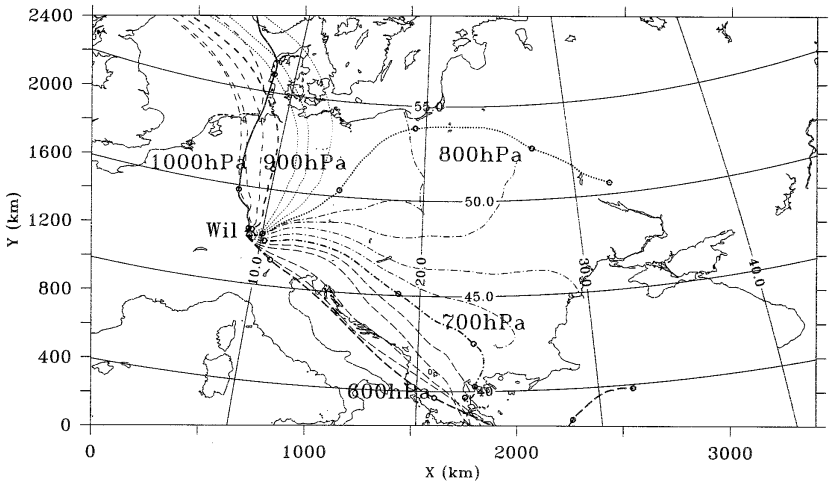

FIG. 7. Isobaric trajectories between the surface and 600 hPa in intervals of 20 hPa, based on ECMWF analyses, starting at 2000 UTC 9 September at Wil, Switzerland. Trajectory positions are marked every 24 h.

The comparison of the first 52 h of isobaric forecast (FT) and analysis trajectories (AT) showed the influence of forecast errors (Figs. 6 and 7). At 1000 hPa and 900 hPa, the FT meandered more than the AT. According to the predicted wind field, the FT turned eastward on the first day and westward on the following night, whereas the AT went straight northward from the beginning. The radial distances LP of the FT end points from the starting point were therefore much smaller than those of the AT (Table 2). The FT at 800 hPa ran eastward and turned to the southeast on the second day. The AT went northeast. The LP of the FT were only slightly longer than the LP of the AT. The errors in the FT at levels above 800 hPa were much larger than those below. According to the predicted wind fields (Figs. 3 and 5), upper air above the Alpine region moved southeast within the frontal zone on the first day and ran around the southern edge of the trough above the eastern Balkan on the second day. The FT at 700 hPa and 600 hPa followed this predicted flow. The respective AT turned southeast on the first day, but as the trough was situated further southwest, the upper flow was much slower than predicted. This resulted after 52 h of trajectory errors of about 1000 km at 700 hPa and nearly 2000 km at 600 hPa (Table 2).

TABLE 2. Comparison of the pathlength (LP) of forecasted and analyzed trajectories, and the absolute horizontal trajectory deviation (AHTD) between forecast and analyzed trajectories after 52 h of travel time.

Pressure level (hPa)	LP forecast (km)	LP analysis (km)	$AHTD_{end}$ (km)
1000	877	910	327
900	502	1498	1338
800	1583	1291	992
700	2674	1644	1039
600	3681	2265	1982

b. Isobaric ensemble trajectories

Considering the synoptic situation during this period, dominated by rather strong westerlies at upper levels (Fig. 3), the high variance of directions of the individual balloon tracks (Fig. 1) is remarkable.

Detailed height information was not available for all balloons. Based on the information of the surface and upper-level geopotential charts, we supposed that balloons that went northward traveled with the flow below 800 hPa, whereas the teams that headed eastward used the upper-level westerlies.

The question arose of whether the trajectory model was able to reproduce the observed variety of tracks. For this purpose, a sample of isobaric trajectories was calculated for pressure levels between the surface and 600 hPa in steps of 20 hPa, based on ECMWF analysis data. The results are shown in Fig. 7. The model produced a variety of trajectories that covered the entire area reached by the balloons. The spread of the trajectories between 800 and 700 hPa especially underlined the complexity of the wind fields and explained the large differences in the balloon tracks.

c. Detailed comparisons

Detailed data were available on the tracks of four balloons (those of teams 1, 3, 6, and 7). By chance, these four tracks differred strongly from each other and gave a good cross section of the whole sample (see Fig. 1), with one balloon heading eastward and the three others northward to northeastward.

A reproduction of the balloon trajectories was attempted by calculating trajectories using the method described in section 3a. In addition to a reference trajectory, we calculated 100 stochastic ensemble trajectories. The ensemble is a sample drawn from the set of possible

trajectory realizations suggested by the trajectory model on the basis of the underlying wind fields and uncertainties of the trajectory calculation. A trajectory ensemble staying close together indicates a rather low uncertainty of the reference trajectory, whereas diverging ensemble trajectories indicate high uncertainty.

The ensemble trajectories were produced to account for two sources of trajectory errors. First, the amplification of trajectory position errors in diffluent wind fields was accounted for by varying the ensemble trajectory starting positions in a circle 100 km in diameter—that is, approximately one grid distance—around the balloon starting point. Second, normally distributed random errors were added to the mean wind speeds at each computational time step to account for interpolation errors. The perturbed wind speeds u_p and v_p were calculated as

$$u_p = u(1 + \lambda_u\sigma_u) \quad (5)$$

and

$$v_p = v(1 + \lambda_v\sigma_v), \quad (6)$$

where u and v are the interpolated mean wind speeds, λ_u and λ_v are random numbers from a standardized Gaussian distribution, and σ_u and σ_v both have values of 7%, a typical magnitude of the relative errors caused by interpolating the horizontal wind components of the ECMWF model fields (Stohl et al. 1995). The ensemble trajectories thus demonstrate the combined effects of interpolation errors and diffluent wind fields, but they do not account for the inherent uncertainties of the wind analyses.

The balloon of team 1 slowly gained height up to 3 km within the first 60 h (Fig. 8). On 12 September, rainy weather twice forced the balloon to sink to about 500 m. On the night of 12–13 September, the balloon once more dropped to 50 m above the Baltic Sea, but rose up to 5 km after dropping ballast before the landing in Latvia.

Beneath 2 km the balloon traveled straight northward. Over these first 200 km, the calculated trajectories and the balloon trajectories were nearly identical. The subsequent northeastward turn of the balloon was also well reproduced by the model. Soon after this turn, however, the trajectory ensemble spread at an increasing rate, indicating a growing uncertainty of the reference trajectory. The ensemble suggested two clusters of highly probable trajectories, one heading northward and turning to the west toward Scandinavia, the other having a tendency toward northeastern Europe, similar to the real balloon track. The area in between these two clusters was only sparsely populated by ensemble members.

After the northeastward turn of the balloon, the deviation between the reference trajectory and the balloon trajectory grew, finally reaching an AHTD of nearly 900 km (RHTD 45%) after 91 h of travel time (Table 3). Nevertheless, the balloon trajectory stayed within the area covered by the ensemble trajectories during all of the flight except for the last 100 km—the AHTD, averaging 258 km over the whole trajectory, (RHTD 26%) was found to be comparatively small (Table 3).

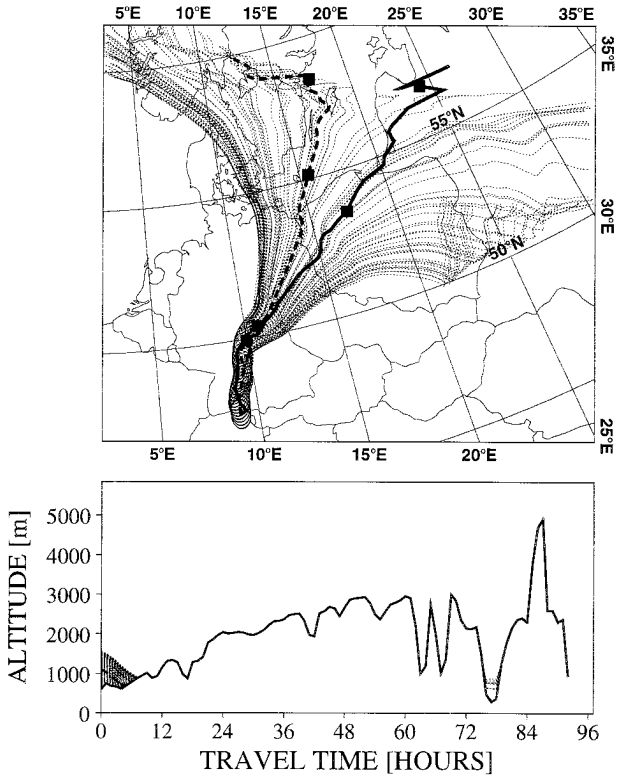

FIG. 8. Balloon track of team 1 (solid line), the respective computed reference trajectory (thick dashed line), and 100 ensemble trajectories (thin dotted lines). Trajectory positions of the balloon and reference trajectory are marked every 24 h. The lower part of the figure shows the time–height profile of the flight. During those parts of the flights in which more than one line is shown, the balloon traveled below the ECMWF topography and the ensemble trajectories were advected along the lowest model level.

Team 3 rose fast after the start and maintained heights of between 2 and 3 km during most of the flight, traveling eastward to Ukraine (Fig. 9). The ensemble trajectories remained close together and, accordingly, the distance between the calculated trajectory and the balloon trajectory was less than 150 km during the whole flight. As the spread of the ensemble trajectories was low, the balloon trajectory was not enveloped by the ensemble trajectories during the first half of the flight, but traveled somewhat to the south. However, later on, the trajectories coincided again. The AHTD were 127 km (RHTD 21%) on average and 180 km (12%) at the end point after 80 h of travel time (Table 3).

Team 6 landed in Denmark, at the westernmost landing position of all the balloons (Fig. 10). The balloon ascended fast, although slower than the team 3 balloon, and traveled northeastward. Then it stayed below 2500 m most of the time, never entering higher layers with westerly winds, and therefore traveled northward. This was well reproduced by the calculated trajectories, with

TABLE 3. Statistical comparison of the calculated and the balloon trajectories for teams 1, 3, 6, and 7. Distance between start and landing position (LR), pathlength (LP), and the meandering factor (MF) of the balloon and respective computed trajectories, mean heights of the flights (h_m), and absolute and relative horizontal deviations between the balloon and computed trajectories (AHTD, RHTD) are shown. For further description, see section 3b.

	Balloon			Computed				Trajectory end		Mean	
Team	LR (km)	LP (km)	MF	LR [km (%)]	LP [km (%)]	MF	h_m (m)	AHTD (km)	RHTD (%)	AHTD (km)	RHTD (%)
1	1587	2040	1.29	1396 (88)	1822 (89)	1.31	1853	874	45	258	26
3	1391	1568	1.13	1277 (92)	1390 (89)	1.09	2378	177	12	127	21
6	932	1137	1.22	953 (102)	1079 (95)	1.13	1687	45	4	2	1
7	883	1013	1.15	975 (110)	1009 (100)	1.03	1641	324	32	106	31

the small ensemble spread indicating high confidence into the reference trajectory. The agreement between the balloon and the reference trajectory was excellent in this case. Although initially outside the narrow band of ensemble trajectories, the AHTD after 46 h of travel time was only 45 km (RHTD 4%). The mean AHTD was 44 km (RHTD 24%).

The track of team 7 was similar to that of team 1, continuously rising to nearly 4 km and traveling to northwestern Poland (Fig. 11). The ensemble trajectories completely enveloped the balloon trajectory. As for team 1, the course of the calculated reference trajectory was west of the balloon track. The mean of the AHTD was 106 km (RHTD 31%), reaching 320 km (32%) at the trajectory end points after 47 h (Table 3).

Summary statistics of these flights are presented in Table 3. The trajectory ranges LR as well as the pathlengths LP of all four teams were excellently reproduced by the model, with a maximum error in length of 12%.

In spite of different courses and heights, the meandering factors for all the balloon trajectories were approximately 1.2. For teams 1 and 3, which traveled at average heights of about 2000 m, the meandering factor of the balloon and the computed trajectories were nearly identical. For teams 6 and 7, which traveled on a lower mean level of about 1600 m, the computed trajectories meandered less than the balloon tracks. This suggests that the lower-level wind fields were more homogeneous in the ECMWF analyses than in reality, probably because of the limited model resolution, especially the coarse representation of topography in the model.

The mean relative deviations between the tracks of

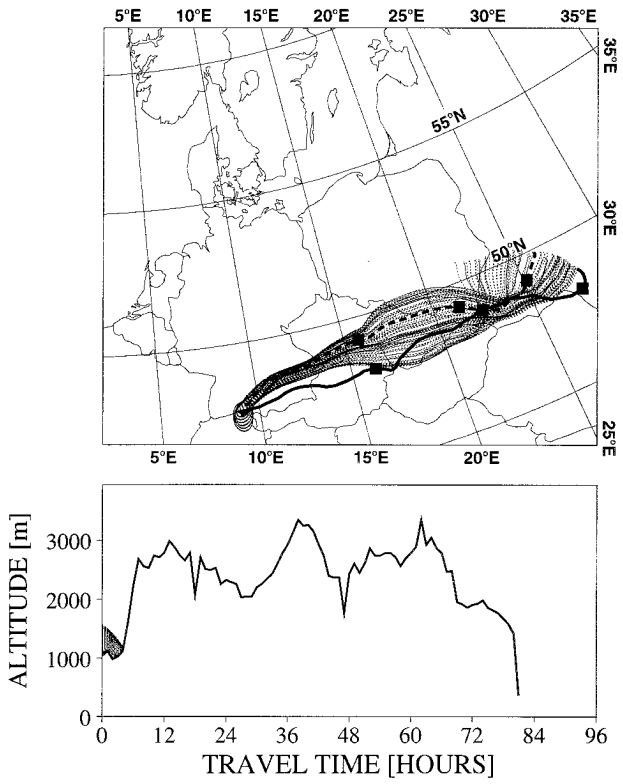

FIG. 9. Same as Fig. 8 but for team 3.

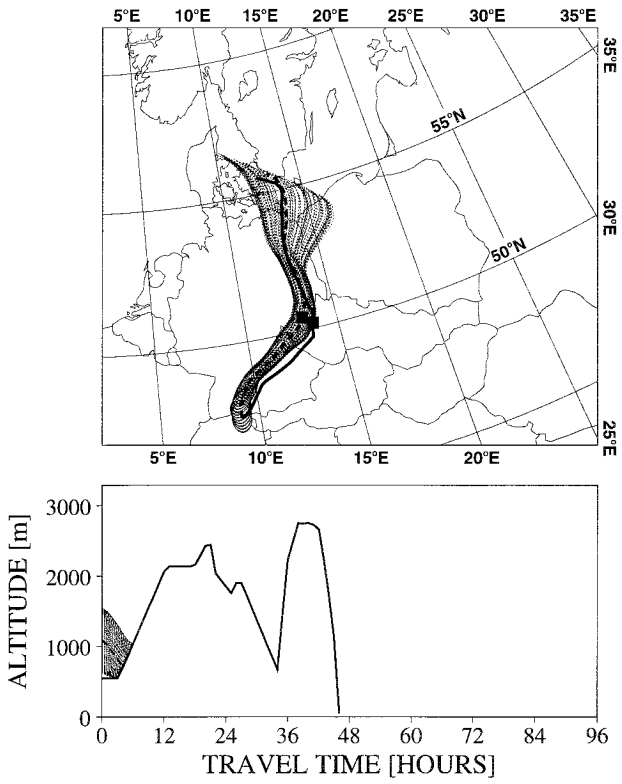

FIG. 10. Same as Fig. 8 but for team 6.

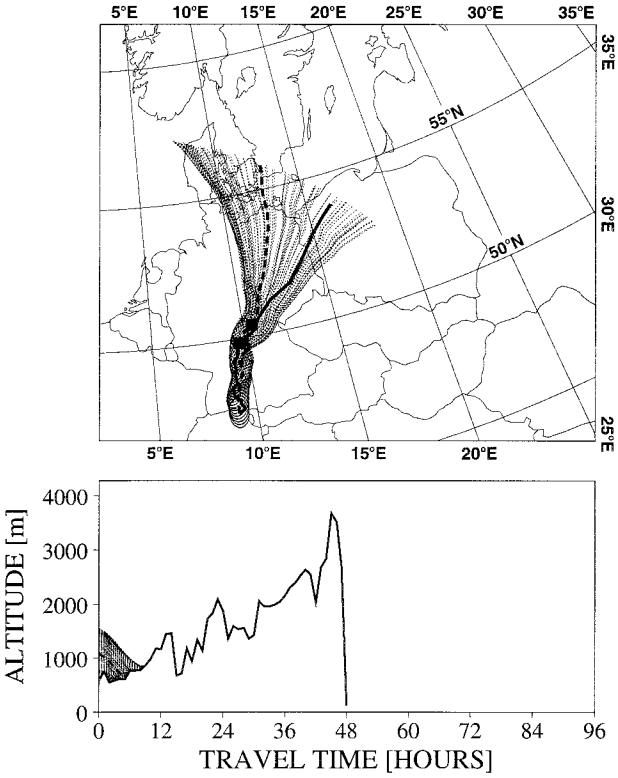

FIG. 11. Same as Fig. 8 but for team 7.

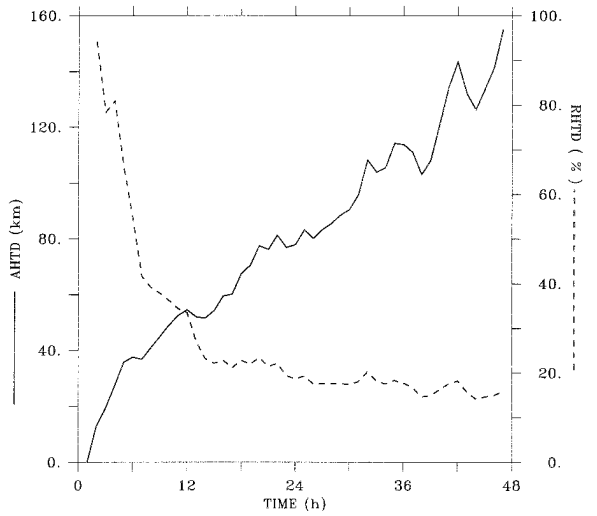

FIG. 12. Mean AHTD and RHTD for balloon and computed trajectories of teams 1, 3, 6, and 7.

teams 1, 3, and 7 and the respective computed trajectories ranged between 21% and 31% and corresponded to the results of other authors (Haagenson et al. 1987 1990; Draxler et al. 1991), while the deviation for team 6 was extremely small. The overall trajectory errors in this case were thus somewhat lower than those reported in other studies.

Absolute and relative deviations as functions of travel time, averaged over the four balloon flights, are shown in Fig. 12. The AHTD increased almost linearly with travel time within the first 46 h, except during the first 15 h, when its increase was stronger. The small fluctuations are not significant because of the small sample. The RHTD decreased rapidly within the first 10 to 15 h and afterward decreased slowly to less than 20%. Similar dependencies of AHTD and RHTD on travel time have been documented in previous studies (e.g., Haagenson et al. 1990).

5. Summary and conclusions

This paper presents a new method for validating long-range trajectory models, namely, comparing gas balloon tracks with calculated trajectories. As balloons are actively changing their height, the FLEXTRA trajectory model was modified to calculate trajectories with a prescribed vertical movement. The major limitation of this method is that balloons are only tracers of horizontal air motions and not of vertical ones. Thus, trajectory uncertainties caused by errors in the vertical wind cannot be assessed. Nevertheless, if balloon data are available, the method provides a cheap and valuable opportunity to validate trajectory models.

Eighteen balloons competed in the Gordon Bennett Cup. All balloons started from the same location and at approximately the same time. Differences in the tracks are therefore only caused by their different time–height profiles. For four of the balloon flights, having durations ranging from 46 to 91 h, detailed tracks were available. They were compared with calculated trajectories based on analyzed wind fields of the ECMWF model.

Major findings of this study are the following.

- The main patterns of the lower and upper pressure fields were forecast reasonably well by the ECMWF model, giving a good qualitative estimation of the wind shear and the mean lower- and upper-level air flow in the present case. Nevertheless, the strong wind shear between 900 and 700 hPa and the location of the trough in the upper pressure field were not predicted correctly, resulting in rather large errors of the forecast trajectories at 900 hPa and above.
- The wind analyses of the ECMWF model were good in this case. Isobaric trajectories calculated at levels from the surface to 600 hPa reproduced the real spread of the balloon tracks. For those four balloons for which detailed tracks were available, the computed trajectory ensemble nearly always enveloped the balloon tracks, indicating that wind analysis errors not accounted for by the ensemble method were small.
- Calculating ensemble trajectories by varying the starting position and accounting for random interpolation errors allowed a detailed assessment of trajectory uncertainty. In those cases in which the ensemble stayed close together, the balloon trajectory also stayed close to the calculated reference trajectory, whereas a spread

of the ensemble trajectories always indicated a growing deviation between the reference and the balloon trajectory. Thus, the ensemble method is strongly recommended for an assessment of trajectory uncertainties.
- The mean absolute horizontal transport deviations between balloon and reference trajectories, averaged over four cases, increased nearly linearly with travel time within the first 46 h, whereas their mean relative horizontal transport deviations decreased rapidly within the first 10–15 h and slowly afterward to less than 20% after 46 h.

Acknowledgments. We thank the Central Institute of Meteorology and Geodynamics in Austria for supporting this study. Thanks go to G. Wotawa for supplying the ECMWF analyses, and special thanks for valuable balloon data go to the pilots W. Eimers, J. Fürstner, J. Höhl, H. Brachtendorf, and G. Stürzlinger, as well as to the ballooning club of Fürstenland, Switzerland. We also thank G. Mahringer and G. Stürzlinger for helpful hints and advice, and P. Seibert and G. Erbes for critical reviews of the manuscript. Comments of three anonymous reviewers were also helpful.

REFERENCES

Artz, R., R. A. Pielke, and J. Galloway, 1985: Comparison of the ARL/ATAD constant level and the NCAR isentropic trajectory analyses for selected case studies. *Atmos. Environ.,* **19,** 47–63.

Doty, K. G., and D. J. Perkey, 1993: Sensitivity of trajectory calculations to the temporal frequency of wind data. *Mon. Wea. Rev.,* **121,** 387–401.

Draxler, R. R., 1991: The accuracy of trajectories during ANATEX calculated using dynamic model analyses versus rawinsonde observations. *J. Appl. Meteor.,* **30,** 1446–1467.

——, 1996: Trajectory optimization for balloon flight planning. *Wea. Forecasting,* **11,** 111–114.

ECMWF, 1995: User guide to ECMWF products 2.1. Meteorological Bulletin M3.2, 71 pp.

Haagenson, P. L., Y. H. Kuo, M. Skumanich, and N. L. Seaman, 1987: Tracer verification of trajectory models. *J. Climate Appl. Meteor.,* **26,** 410–426.

——, K. Gao, and Y.-H. Kuo, 1990: Evaluation of meteorological analyses, simulations, and long-range transport using ANATEX surface tracer data. *J. Appl. Meteor.,* **29,** 1268–1283.

Kahl, J. D. W., 1996: On the prediction of trajectory model error. *Atmos. Environ.,* **30,** 2945–2957.

——, and P. J. Samson, 1986: Uncertainty in trajectory calculations due to low resolution meteorological data. *J. Climate Appl. Meteor.,* **25,** 1816–1831.

——, J. M. Harris, G. A. Herbert, and M. P. Olson, 1989: Intercomparison of three long-range trajectory models applied to Arctic haze. *Tellus,* **41B,** 524–536.

——, R. C. Schnell, P. J. Sheridan, B. D. Zak, H. W. Church, A. S. Mason, J. L. Heffter, and J. M. Harris, 1991: Predicting atmospheric debris transport in real-time using a trajectory forecast model. *Atmos. Environ.,* **25A,** 1705–1713.

Klug, W., 1992: *Evaluation of Long-Range Atmospheric Transport Models Using Environmental Radioactivity Data from the Chernobyl Release.* Elsevier Science Publishing, 366 pp.

Knudsen, B. M., and G. D. Carver, 1994: Accuracy of the isentropic trajectories calculated for the EASOE campaign. *Geophys. Res. Lett.,* **21,** 1199–1202.

Kuo, Y.-H., M. Skumanich, P. L. Haagenson, and J. S. Chang, 1985: The accuracy of trajectory models as revealed by the observing system simulation experiments. *Mon. Wea. Rev.,* **113,** 1852–1867.

Martin, D., G. Bergametti, and B. Strauss, 1990: On the use of the synoptic vertical velocity in trajectory model: Validation by geochemical tracers. *Atmos. Environ.,* **24A,** 2059–2069.

Maryon, R. H., and C. C. Heasman, 1988: The accuracy of plume trajectories forecast using the U.K. Meteorological Office operational forecasting models and their sensitivity to calculation schemes. *Atmos. Environ.,* **22,** 259–272.

McQueen, J. T., and R. R. Draxler, 1994: Evaluation of model back trajectories of the Kuwait oil fires smoke plume using digital satellite data. *Atmos. Environ.,* **28,** 2159–2174.

Merrill, J. T., R. Bleck, and L. Avila, 1985: Modeling atmospheric transport to the Marshall Islands. *J. Geophys. Res.,* **90,** 12 927–12 936.

Miller, J. M., 1987: The use of back air trajectories in interpreting atmospheric chemistry data: A review and bibliography. NOAA Tech. Memo. ERL ARL-155, 28 pp. [Available from Air Resources Laboratory, 8060 13th St., Silver Spring, MD 20910.]

Pack, D. H., G. J. Ferber, J. L. Heffter, K. Telegadas, J. K. Angell, W. H. Hoecker, and L. Machta, 1978: Meteorology of long-range transport. *Atmos. Environ.,* **12,** 425–444.

Petterssen, S., 1940: *Weather Analysis and Forecasting.* McGraw-Hill, 503 pp.

Pickering, K. E., A. M. Thompson, D. P. McNamara, and M. R. Schoeberl, 1994: An intercomparison of isentropic trajectories over the South Atlantic. *Mon. Wea. Rev.,* **122,** 864–879.

Reiff, J., G. S. Forbes, F. T. M. Spieksma, and J. J. Reynders, 1986: African dust reaching northwestern Europe: A case study to verify trajectory calculations. *J. Climate Appl. Meteor.,* **25,** 1543–1567.

Reisinger, L. M., and S. F. Mueller, 1983: Comparisons of tetroon and computed trajectories. *J. Climate Appl. Meteor.,* **22,** 664–672.

Rolph, G. D., and R. R. Draxler, 1990: Sensitivity of three-dimensional trajectories to the spatial and temporal densities of the wind field. *J. Appl. Meteor.,* **29,** 1043–1054.

Seibert, P., 1993: Convergence and accuracy of numerical methods for trajectory calculations. *J. Appl. Meteor.,* **32,** 558–566.

Stocker, R. A., R. A. Pielke, A. J. Verdon, and J. T. Snow, 1990: Characteristics of plume releases as depicted by balloon launchings and model simulations. *J. Appl. Meteor.,* **29,** 53–62.

Stohl, A., 1996a: On the use of trajectories for establishing source–receptor relationships of air pollutants. Ph.D. dissertation, University of Vienna, 189 pp. [Available from University of Vienna, Institute of Meteorology, Hohe Warte 38, 1190 Vienna, Austria.]

——, 1996b: Trajectory statistics—A new method to establish source–receptor relationships of air pollutants and its application to the transport of particulate sulfate in Europe. *Atmos. Environ.,* **30,** 579–587.

——, G. Wotawa, P. Seibert, and H. Kromp-Kolb, 1995: Interpolation errors in wind fields as a function of spatial and temporal resolution and their impact on different types of kinematic trajectories. *J. Appl. Meteor.,* **34,** 2149–2165.

——, K. Baumann, G. Wotawa, M. Langer, B. Neininger, M. Piringer, and H. Formeyer, 1997: Diagnostic downscaling of large-scale wind fields to compute local-scale trajectories. *J. Appl. Meteor.,* in press.

Walmsley, J. L., and J. Mailhot, 1983: On the numerical accuracy of trajectory models for long-range transport of atmospheric pollutants. *Atmos.–Ocean,* **21,** 14–39.